J. Fluid Mech. (1985), *vol.* 150, *pp.* 233–251
Printed in Great Britain

Computations of overturning waves

By A. L. NEW†, P. McIVER AND D. H. PEREGRINE
School of Mathematics, University of Bristol, Bristol BS8 1TW, England

(Received 25 August 1983 and in revised form 31 July 1984)

The numerical method of Longuet-Higgins & Cokelet (1976), for waves on deep water, is extended to account for a horizontal bottom contour, and used to investigate breaking waves in water of finite depth. It is demonstrated that a variety of overturning motions may be generated, ranging from the projection of a small-scale jet at the wave crest (of the type that might initiate a spilling breaker) to large-scale plunging breakers involving a significant portion of the wave. Although there seems to be a continuous transition between these wave types, a remarkable similarity is noticed in the overturning regions of many of the waves.

Three high-resolution computations are also discussed. The results are presented in the form of interrelated space-, velocity- and acceleration-plane plots which enable the time evolution of individual fluid particles to be followed. These computations should be found useful for the testing of analytical theories, and may also be applied, for example, to studies of slamming forces on shipping and coastal structures.

1. Introduction

Breaking waves have been classified into four main types by Galvin (1968). Two of his categories clearly fall under the heading of 'overturning' waves. These are the plunging breaker, in which a symmetric wave steepens until a large-scale jet is thrown forward from the crest region, and the collapsing breaker, an abbreviated form of the plunger, which overturns some way down the forward face. A third type, the spilling breaker, is a near-symmetric wave distinguished by a turbulent layer of foaming water on its forward face. Although this cannot be described solely in terms of irrotational flow, observations suggest that the initial stages of spilling may involve a very localized jet at the wave crest. These three breaker types seem to form a single family in which there is a continuous variation in the extent and nature of the overturning region. (The fourth type described by Galvin, the surging breaker, occurs only on steep beaches and is beyond the scope of the present work.) A modification to finite depth of the deep-water method of Longuet-Higgins & Cokelet (1976) is used to investigate this range of breaking waves, and, although the calculations are for flow over a horizontal bottom, a beach-slope parameter is derived and discussed.

The fluid mechanics of the early stages of the overturning process, before the development of a prominent jet, is investigated by Peregrine, Cokelet & McIver (1980). These authors classify three regions of particular interest: high particle velocities near the wave crest, high accelerations on the forward face, and low accelerations on the rear face. (This latter region is interpreted as providing support for the high pressure gradients that are required to accelerate fluid particles into the jet.)

† Present address: Institute of Oceanographic Sciences, Crossway, Taunton, Somerset TA1 2DW, England.

However, in order to follow the motion into the more advanced stages of breaking, it is necessary to increase the number of surface particles used in the calculations. An important aspect of the present paper is the discussion of three such high-resolution examples, two of which can be followed until immediately before the 'touchdown' of the jet on the forward face. Computations such as these should be found useful for the testing of analytical theories (for instance, Longuet-Higgins (1980) suggests that the motion near the jet tip may be described by a rotating form of the Dirichlet hyperbola), and, although the knowledge that large accelerations may occur in breaking waves is not new, we know of no other calculations of the late stages of the overturning motion which are given in similar detail. The examples in the present paper enable particle trajectories to be simultaneously followed in the space, velocity and acceleration planes, and such a detailed knowledge of the wave kinematics may be of use to those interested in the design of shipping or coastal structures.

Section 2 of the present paper describes the numerical methods which were used, and in particular shows how the deep-water method of Longuet-Higgins & Cokelet (1976) may be simply extended to account for a horizontal bottom at finite depth. The accuracy of the computations (an important consideration) is then investigated in §3. In §4 we present a set of eight waves in shallow water, which are forced to break by perturbing the position of the bed, and a beach-slope parameter is derived. Section 5 then describes the high-resolution computations, one of which is in deep water, and indicates that accelerations as high as five or six times that due to gravity may occur beneath the overturning wave crest. Finally, in §6 a remarkable similarity between the overturning regions of many of the waves is noted.

2. Numerical technique

This section presents details of the methods used for the calculation of waves in water of both infinite and finite uniform depth.

For the deep-water case, the computations use the boundary-integral technique of Longuet-Higgins & Cokelet (1976). The two-dimensional motion is assumed to be spatially periodic and such that a harmonic velocity potential exists, and units of time and length are chosen so that the wavelength and the acceleration due to gravity are $\lambda = 1$ and $g = 1$ respectively. The physical z-plane is mapped to a computational ζ-domain using the transformation

$$\zeta = \mathrm{e}^{-\mathrm{i}2\pi z}, \tag{2.1}$$

under which one wavelength of the free surface is mapped to a closed contour (C_1 in figure 1). A finite number N of computational particles are then placed on C_1, and we suppose that their positions and ϕ-values are known at some time t_0. If, as in figure 1, (n, s) represents a coordinate system which is locally normal and tangential to the free surface (s being the arclength along C_1 from some arbitrary origin), then the tangential particle velocities $\partial\phi/\partial s$ are simply evaluated by considering adjacent particles and differentiating along the surface. By applying Green's third identity to the fluid volume, a Fredholm integral equation of the first kind for the unknown normal velocity $\partial\phi/\partial n$ is derived in which the Green's function is a simple logarithmic singularity. This integral equation is approximated by a matrix system, which is numerically inverted to find $\partial\phi/\partial n$ at the nodal points. The positions of, and ϕ-values at, these computational particles are then integrated to the next time level $t_0 + \delta t$ using the kinematic and dynamic free-surface boundary conditions in conjunction with a fourth-order Adams–Bashforth–Moulton technique (with starting values given by a

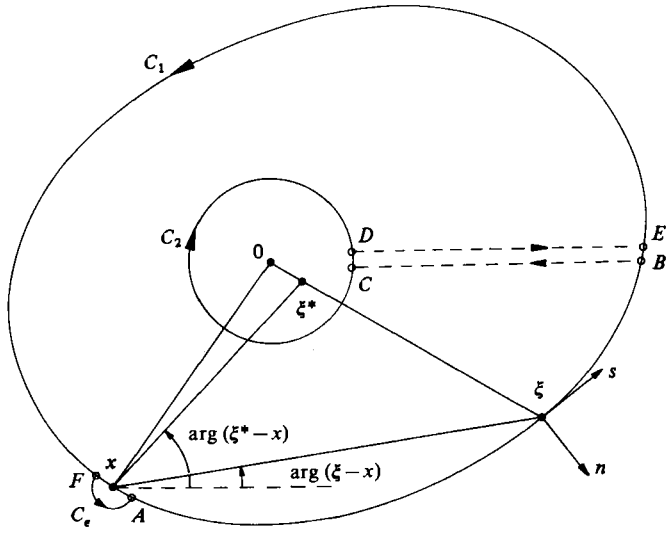

FIGURE 1. The transformed (computational) plane, showing the construction of the Green's function. C_1 represents one wavelength of the free surface, and C_2 is the bed.

Runge–Kutta procedure). Thus the fluid flow, starting from given initial conditions, can be followed forward through time.

The calculations for the finite-depth case use a simple extension of this procedure to model a horizontal bottom, taken as $y = -d$, and full details are as given in New (1983*a*). Under the transformation (2.1), the bottom becomes a circle of radius $r_0 = \mathrm{e}^{-2\pi d}$ (see C_2 in figure 1), and the problem reduces to the derivation and solution of an integral equation for $\partial\phi/\partial n$, as for the deep-water method.

Suppose $\boldsymbol{x}$ is fixed at some point in the fluid domain, while $\boldsymbol{\xi}$ is allowed to vary. We seek a Green's function $G(\boldsymbol{x};\boldsymbol{\xi})$ and its 'complement' $\alpha(\boldsymbol{x};\boldsymbol{\xi})$ satisfying

$$\nabla^2 G = 0, \quad \nabla^2 \alpha = 0 \tag{2.2a, b}$$

for all points in the fluid domain, except $\boldsymbol{\xi} = \boldsymbol{x}$, with the boundary conditions

$$\frac{\partial G}{\partial n}(\boldsymbol{x};\boldsymbol{\xi}) = 0, \quad \boldsymbol{\xi} \text{ on } C_2; \quad \frac{\partial \alpha}{\partial s}(\boldsymbol{x};\boldsymbol{\xi}) = 2\pi \frac{\partial G}{\partial n}(\boldsymbol{x};\boldsymbol{\xi}), \quad \boldsymbol{\xi} \text{ on } C_1. \tag{2.2c, d}$$

In the deep-water case, the bottom contour vanishes and the Green's function is given by a simple logarithmic singularity at $\boldsymbol{\xi}$. For the finite-depth case, however, it is found necessary to place an image singularity at

$$\boldsymbol{\xi}^* = r_0^2 \boldsymbol{\xi}/|\boldsymbol{\xi}|^2, \tag{2.3}$$

which is the geometrical reflection of $\boldsymbol{\xi}$ in C_2. The Green's function is thus given by

$$G(\boldsymbol{x};\boldsymbol{\xi}) = \frac{1}{2\pi} \ln R(\boldsymbol{x};\boldsymbol{\xi}), \tag{2.4a}$$

where

$$R(\boldsymbol{x};\boldsymbol{\xi}) = |\boldsymbol{\xi}-\boldsymbol{x}||\boldsymbol{\xi}^*-\boldsymbol{x}|, \tag{2.4b}$$

and

$$\alpha(\boldsymbol{x};\boldsymbol{\xi}) = \arg(\boldsymbol{\xi}-\boldsymbol{x}) - \arg(\boldsymbol{\xi}^*-\boldsymbol{x}), \tag{2.4c}$$

and its construction is as indicated in figure 1. The minus sign in (2.4*c*) is due to the right-handed system (n, s) at $\boldsymbol{\xi}$ being 'mirrored' by a left-handed set at $\boldsymbol{\xi}^*$. Further,

it is clear that an image singularity, of unit negative strength and placed at the origin, may be added to the Green's function as given above, so that, if we then consider the limit of increasing depth, the singularity at $\boldsymbol{\xi}^*$ will be cancelled and the deep-water Green's function returned.

The integral equation for $\partial\phi/\partial n$ is now derived by integrating Green's third identity over the fluid volume, suitably indented to include a semicircular contour, C_ϵ, of vanishingly small radius at $\boldsymbol{x}$ (i.e. $ABCDEFA$ in figure 1). Remembering that the normal derivatives of both G and ϕ vanish on C_2, we deduce that

$$\oint_{C_1} \ln R(\boldsymbol{x};\boldsymbol{\xi}) \frac{\partial\phi}{\partial n}(\boldsymbol{\xi})\,\mathrm{d}s = -\int_{C_1} \alpha(\boldsymbol{x};\boldsymbol{\xi}) \frac{\partial\phi}{\partial s}(\boldsymbol{\xi})\,\mathrm{d}s, \tag{2.5}$$

where the integral on the right-hand side is principal in the sense that the contribution from C_ϵ is not included.

This integral equation involves only the free surface C_1, so that computational particles do not need to be placed on the bottom contour C_2. It is of exactly the same form as that derived by Longuet-Higgins & Cokelet (1976) for waves on water of infinite depth, and is solved in a similar manner. Thus a simple extension to the case of a horizontal bottom is achieved.

3. Accuracy of the computations

The computations reported by Longuet-Higgins & Cokelet (1976) exhibited a 'sawtooth' instability, which was overcome by using a suitable smoothing technique. The same method is applied to suppress similar instabilities in the computations described in the present paper, and a number of tests have been made in order to assess the accuracy of the resulting technique.

Methods are available (Cokelet 1977; Rienecker & Fenton 1981) for the accurate calculation of steadily progressing waves in water of both infinite and finite uniform depth. Following the time evolution of such a wave over one period gives results that are visually indistinguishable from the initial wave (displaced horizontally by the correct amount) for all of the depths of water used in this paper. (Note that the breaking events described in §§4 and 5 all occur on a timescale of less than one wave period.)

A more stringent test, however, is provided by a comparison with calculations of overturning waves made using the alternative numerical method of Vinje & Brevig (1981). Though this is again a boundary-integral technique, it is sufficiently different from that used for the present work to make a comparison worth while (for example the integral equation has a $1/|\boldsymbol{x}-\boldsymbol{\xi}|$-type singularity rather than the $\ln|\boldsymbol{x}-\boldsymbol{\xi}|$ factor described in §2). These authors have kindly supplied numerical results for the motion developing from a first-order Stokes wave. Such a wave does not satisfy the surface boundary conditions for steady motion and, for a sufficiently large amplitude, the free surface overturns. A comparison for a deep-water wave has previously been made by McIver & Peregrine (1981). Here, however, a comparison is made for a calculation on water of mean depth $d = 0.1333$. The initial free-surface profile and velocity potential are given by

$$y_s(x) = a_0 \cos 2\pi x \tag{3.1a}$$

and

$$\phi(x, y_s) = a_0(2\pi)^{-\frac{1}{2}} \sin 2\pi x, \tag{3.1b}$$

where the amplitude $a_0 = 0.0667$. The comparison of the two calculations, both using $N = 59$ free-surface particles, is made in figure 2. The wave profiles, upon which the

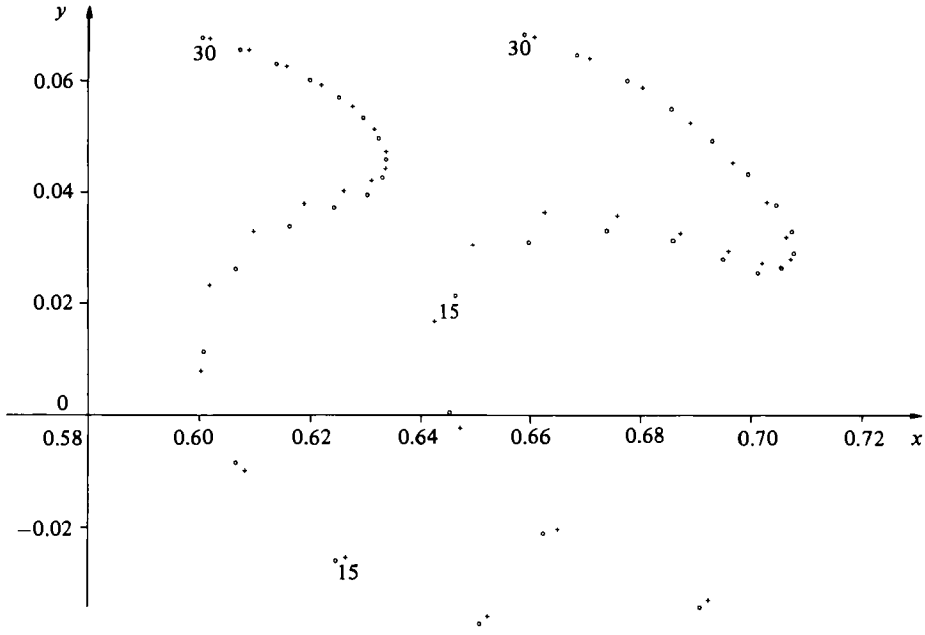

FIGURE 2. Comparison of the present method (○) with that of Vinje & Brevig (1981, +) for a breaking sine wave. The profiles are at times $t = 1.10$ and $t = 1.25$.

particle numbers are indicated, are displayed for times $t = 1.10$ and 1.25 (in the present units the wave period is approximately $(2\pi)^{\frac{1}{2}} \approx 2.51$), and the largest discrepancies occur on the underside of the overhanging jet. The particles here have just passed through the region of highest (surface) accelerations (near the vertical tangent on the forward face, see §5), and so we might expect them to have incurred the largest errors. However, the overall agreement is good and the small differences in the profiles are an indication of the likely errors in both methods.

In §4 details are presented of overturning waves calculated with $N = 60$ free-surface particles. Further examples described in §5 were calculated using an effective value of $N = 180$. All of these computations (in deep and finite-depth water) are thought to be of a similar accuracy and the following discussion of a single case is taken as representative. The example chosen is that labelled 'wave 1' in §4, and the profile at time $t = 1.35$ is shown in figure 3. Computations with both 60 and 180 points are shown, but for the latter only every third particle is plotted: these should coincide with the 60-point calculation, to which the particle numbering refers. Although both profiles are smooth and exhibit no visual evidence of numerical failure, further investigation reveals that the velocities of the particles near the jet tip (i.e. particles 25–38 in the 60-point calculation, and those equivalent to the range 27–33 for the higher-resolution example) are developing some irregularity at this time. Nevertheless, the differences in the positions of the two sets of particles are significantly smaller than those in the above comparison with the method of Vinje & Brevig, and indicate the accuracy of the present numerical technique.

The computation of wave 1 with $N = 60$ free-surface particles breaks down at about time $t = 1.40$, whereas the higher-resolution example can be followed until the jet touches the forward face of the wave, near time $t = 1.62$. The onset of the eventual numerical breakdown is indicated in figure 4, which shows the time variation of two

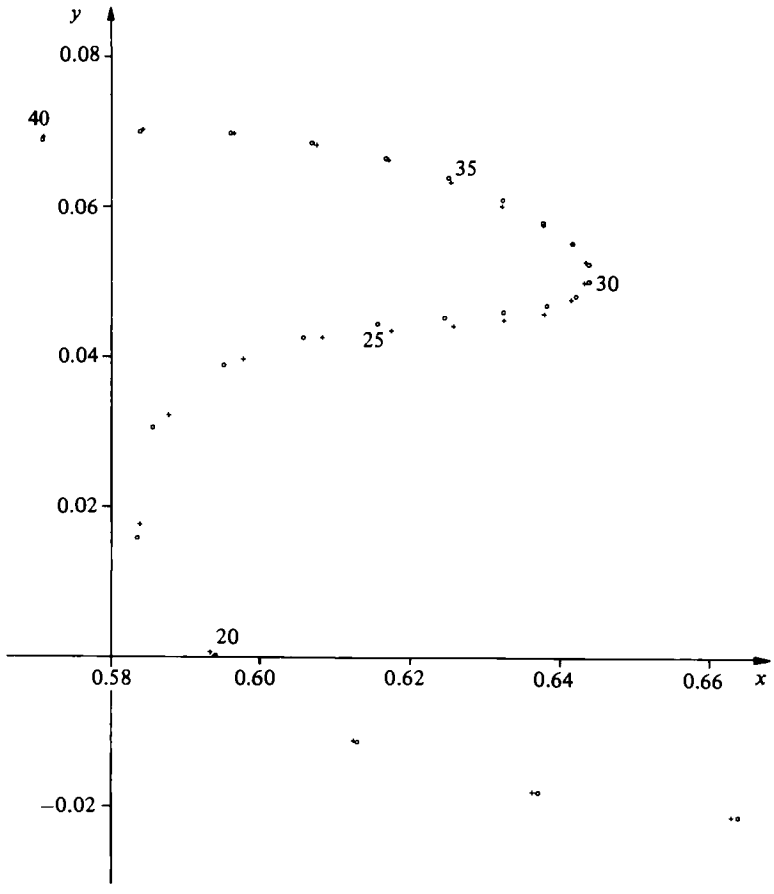

FIGURE 3. Comparison between the 60-point (+) and 180-point (○) calculations of wave 1 at time $t = 1.35$.

integral properties of the wave that are theoretically constant. $E(t)$ is the total (kinetic + potential) energy (per unit span) in one wavelength, which should remain equal to its value E_0 at time $t = 0$, and $\bar{y}(t)$ is the mean level of the free surface, which is initially chosen to be zero. (Mass conservation is automatically ensured by the use of a supplementary condition when solving the integral equation.) The 60-point and the 180-point calculations are both shown. (Note that, for the higher-resolution example, the flow is followed until shortly before time $t = 1.00$ using only 90 free-surface particles, whereupon a further set of 90 particles is interpolated, as described in §5. The broken lines in figure 4 represent the continuation of the 90-point calculation, and we remark that the full set of 180 particles is implemented before the 90-point computation becomes inaccurate.) The errors in the higher-resolution example are typically an order of magnitude less than those obtained when using 60 particles, which is consistent with being able to follow the former calculation further in time. Indeed, the final breakdown of these two computations seems to occur when the respective errors in $E(t)$ (and $\bar{y}(t)$) reach approximately the same level, 10^{-5} (and 10^{-4}).

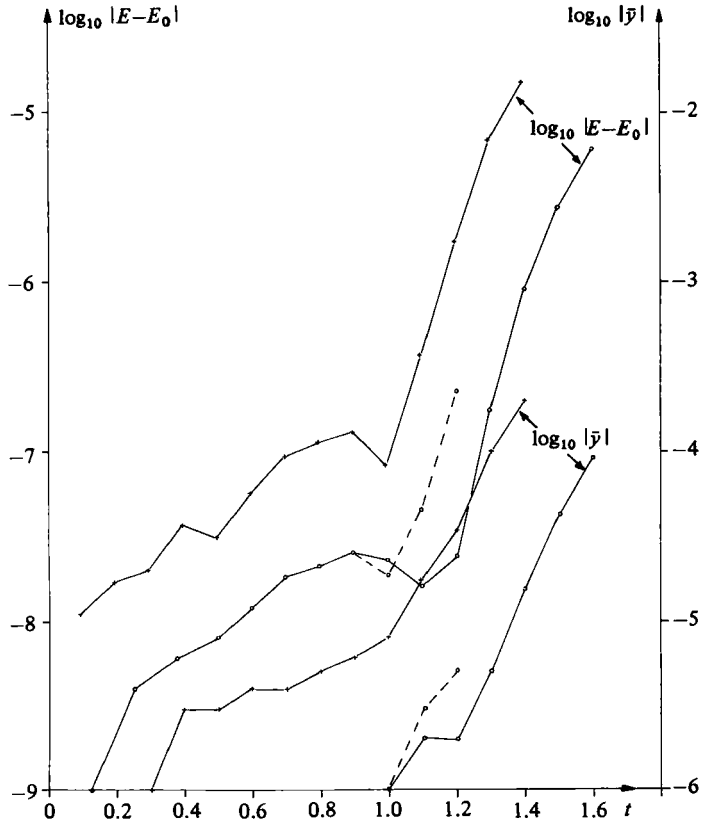

FIGURE 4. Time variation of the total wave energy $E(t)$ and mean level $\bar{y}(t)$, for the 60-point (+) and 180-point (○) calculations of wave 1. The broken line represents the continuing 90-point computation.

4. Waves in water of finite depth

Eight examples of overturning waves in water of finite depth are now presented. These are labelled waves 1–8 and are shown (near to time $t = t_H$, defined below) in figures 5(*a–h*) respectively. Each was computed with 60 free-surface particles, the crest being initially at $x = 0$. The overturning motion is initiated by a 'depth perturbation', such that a wave of initial height H_0, which would progress without change of form on fluid of some mean depth d_0, is instead computed on a depth d (where usually $d < d_0$). Physically, the motion may be considered to result from an initial impulse at the level $y = -d$, which forces the perturbed bottom to become a streamline, and instantaneously changes the complete velocity field. The parameters corresponding to these eight waves are presented in table 1. Here t_V and t_H are respectively the times of the first occurrence of a vertical tangent to the wave profile and of a horizontal tangent beneath the projected jet. Because of the poor numerical resolution of the jet in some of these examples (e.g. see waves 4 and 7 in figure 5), the values of t_H given are only approximate. The 'length' S of the jet at time $t = t_H$ is defined to be the horizontal distance between the jet tip and the vertical tangent beneath the overturning crest. A measure of the overturning time of the wave is given by $T \equiv t_H - t_V$, and the parameter $U \equiv S/T$ is then taken to be representative of the

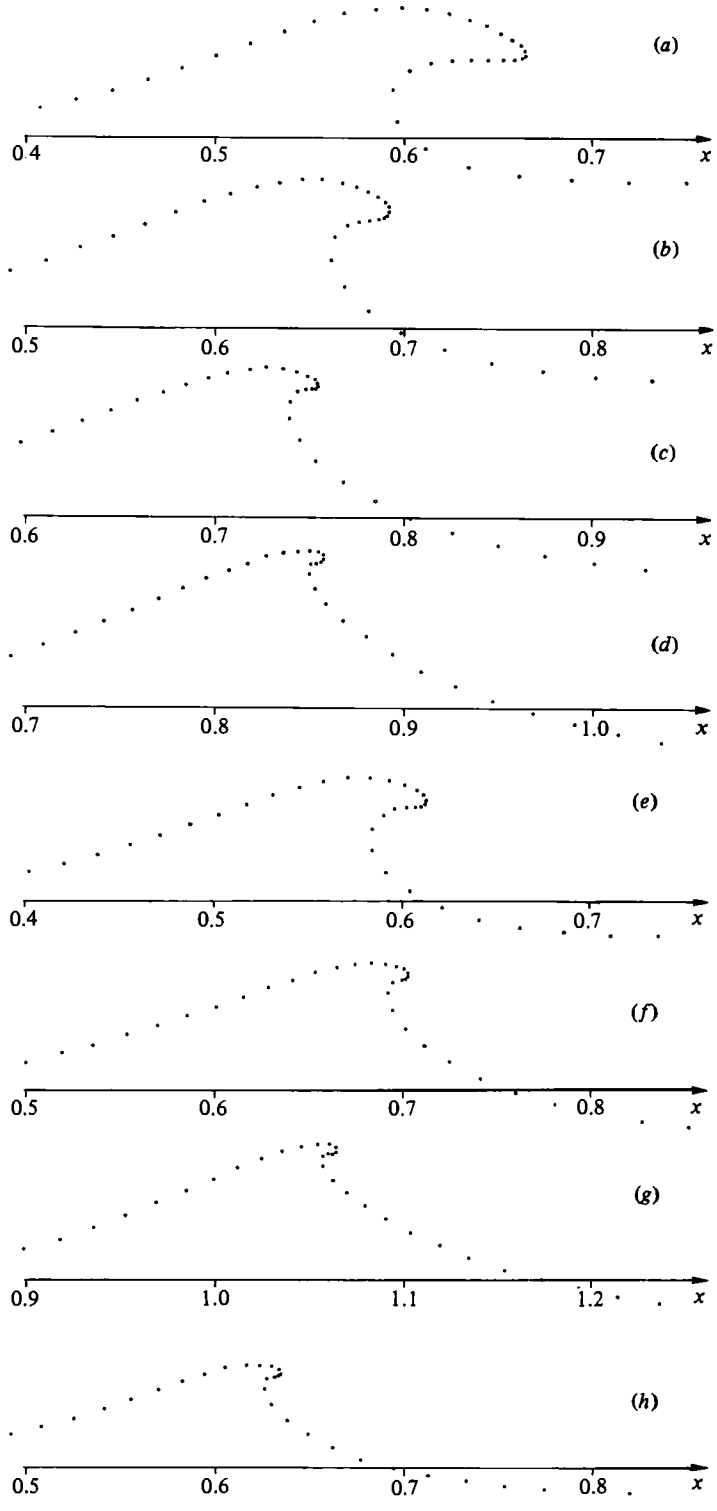

FIGURE 5. A variety of breaking waves in water of finite depth, near time $t = t_H$. Waves 1–8 are shown in (*a*)–(*h*) respectively, and the corresponding parameters are given in table 1.

Wave	d_0	d	H_0	H_b	t_V	t_H
1	0.200	0.070	0.110	0.0881	1.038	1.388
2	0.200	0.100	0.110	0.1104	1.263	1.525
3	0.200	0.132	0.110	0.1125	1.538	1.713
4	0.200	0.165	0.110	0.1132	1.900	2.013
5	0.150	0.070	0.085	0.0808	1.225	1.450
6	0.150	0.100	0.085	0.0928	1.615	1.750
7	0.150	0.132	0.085	0.0952	2.625	2.740
8	0.105	0.070	0.060	0.0706	1.675	1.800

Wave	T	S	U	x_b	m
1	0.350	0.0707	0.202	0.460	0.283
2	0.262	0.0309	0.118	0.547	0.183
3	0.175	0.0168	0.096	0.656	0.104
4	0.113	0.0076	0.067	0.796	0.044
5	0.225	0.0296	0.132	0.495	0.162
6	0.135	0.0110	0.081	0.638	0.078
7	0.115	0.0079	0.069	1.005	0.018
8	0.125	0.0088	0.070	0.582	0.060

TABLE 1. Parameters for the finite-depth waves of §4

speed at which the jet is ejected from the forward face of the wave. Finally, H_b and x_b are the wave height and crest position at 'breaking' (taken as $t = t_V$), and m is an 'equivalent' beach slope, discussed later. The initial free-surface elevation and velocity potential for these waves were calculated using the method of Rienecker & Fenton (1981).

Figure 5 shows a wide variety of breakers, ranging from the strongly plunging wave 1 to the much weaker wave 4, in which near-symmetry is retained between the forward and rear faces. (In this figure the vertical scale is the same as the horizontal (which is measured in units of wavelength), and the x-axis lies in the mean level of the free surface.) In view of the difficulty of choosing appropriate length- and timescales for the overturning motion, perhaps the 'type' of an overturning wave (as described in §1) should depend not so much on the size of the jet region as on the overall asymmetry in the wave. On this basis, we classify waves 1, 2 and 5 as 'plunging', waves 3, 6 and 8 as 'intermediate', and waves 4 and 7 as 'spilling'. These examples do not include any 'collapsing' breakers, possibly because the necessary situation of a steep beach cannot be well modelled by a depth perturbation, however severe.

For those waves having the same unperturbed depth and initial wave height, we see from table 1 and figure 5 that, as the depth perturbation becomes more severe, the overturning time, jet size, and asymmetry of the wave all show a regular increase. These smooth transitions indicate that 'spillers' and 'plungers' can be considered as members of a single family of breaking waves with a continuously varying 'breaker type'.

However, the question now arises as to how realistic the depth perturbation is as a mechanism for generating overturning waves. For instance: can the motion be related to a wave travelling up a plane beach of some 'equivalent' slope m? Consider the initial depth perturbation to be equivalent to a uniform decrease in water depth from d_0 to d between $x = 0$ and $x = x_b$, with a constant depth thereafter. Then, if

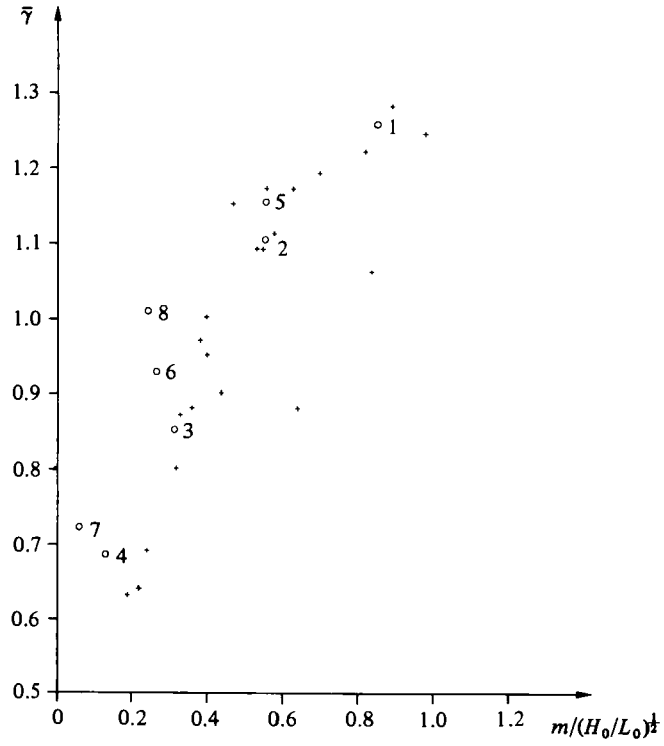

FIGURE 6. A test of the beach-slope parameter m: +, experimental points of Bowen *et al.* (1968); ○, points corresponding to the present computations.

it is assumed that after time $t = t_V$ the wave is committed to breaking in a definite way such that the ensuing motion is little affected by any further changes in the depth, the flow may be similar to that occurring on a beach of slope

$$m = (d_0 - d)/x_b, \tag{4.1}$$

values of which are given in table 1.

The relevance of this parameter is now tested by comparison with the work of Bowen, Inman & Simmons (1968). They use the formula that, for waves incident on a plane sloping beach which are 'breaking' (i.e. at or after time $t = t_V$), the crest-to-trough wave height may be given approximately by

$$H = \gamma(h + \bar{\eta}), \tag{4.2}$$

where γ is a constant, h is the local undisturbed water depth and $\bar{\eta}$ is the wave-induced set-up or set-down. They conducted a number of laboratory experiments in which plunger-generated waves were incident upon plane concrete beaches, and plotted $\bar{\gamma}$ (the average value of γ, for a particular wave, taken over readings from several positions) against (beach slope)$/(H_0/L_0)^{\frac{1}{2}}$, where H_0/L_0 is the steepness of the related deep-water wave. The results appearing in figure 7 of their paper are reproduced in the present figure 6. From (4.2) let us now take $\bar{\gamma}$ for the computational waves as the value of γ at time $t = t_V$, and write

$$\bar{\gamma} = H_b/d, \tag{4.3}$$

where H_b and d are as given in table 1. If we also take the beach slope, as m, and the deep-water steepness, as H_0 (assuming $L_0 = 1$), from this table, the corresponding points for the eight numerical waves of this section may also be plotted. It is apparent from this figure that the numerical results are in general agreement with the experimental values, so that the proposed beach-slope parameter does seem to have some relevance.

The computations described in the present section, using $N = 60$ free-surface particles, generally fail shortly after time $t = t_H$. The investigation of the later stages of overturning requires improvement in the accuracy of the solution by increasing the value of N, as indicated in §3. The detailed results of such calculations are now presented.

5. High-resolution computations

In order to discuss the physically important quantities in a breaking wave (such as velocity and acceleration) during the advanced stages of jet development, the results of three computations are now presented for which there were effectively 180 computational particles in the free surface. (That is, for example, 90 particles were used initially, then, at some time (usually near $t = t_V$) before any significant loss of accuracy occurred, a further set of 90 particles was interpolated. The calculation then proceeded using all 180 particles.) Two of these computations are recalculations of waves 1 and 3 of §4. The third is in deep water and the initial conditions represent a sine wave of amplitude $a_0 = 0.0866$ (see (3.1)). This computation will be labelled wave 9. The purpose of these calculations is primarily to investigate the late stages of the overturning process and the following presentation covers only the interesting period during which the jet is ejected. The fluid mechanics of the earlier development of breaking waves is, as remarked in §1, discussed by Peregrine *et al.* (1980).

For each of the computations a number of specific times are selected for the presentation of results, as follows:

wave 1: $t = 1.150, 1.250, 1.350, 1.452, 1.552$;
wave 3: $t = 1.560, 1.620, 1.680, 1.740, 1.800$;
wave 9: $t = 1.191, 1.316, 1.441, 1.567$.

In each example, the wavelength considered lies initially between $x = 0$ and $x = 1$, with the wave crest at $x = 0$. The profiles for waves 1, 3 and 9 are shown in figures 7 (*a–c*) respectively, and are plotted using the complete set of 180 particles, although for clarity only every fifth is shown. Some of the particles are numbered near the earliest profiles, and the corresponding spatial trajectories are indicated by broken lines. In each case the particles in the jet tip remain there and appear, from a consideration of the acceleration-plane diagrams, to be almost in free fall, so that during the late stages of overturning the jet tip is little influenced by the rest of the wave. It is also observed that the particles near the position of maximum elevation (e.g. particle 110 in wave 9) remain in that region, and that most of the particles entering the jet do so from the forward face of the wave (e.g. follow particles 40–65 for wave 9).

Although the computations for waves 1 and 9 can be continued until the 'touchdown' of the jet onto the forward face, that for wave 3 fails at an earlier time, shortly after the profile shown last in figure 7 (*b*). This is presumably because of the smaller scale of the overturning region, with the correspondingly high surface curvatures resulting in a loss of numerical resolution.

The time evolution of the velocities of typical computational particles is presented

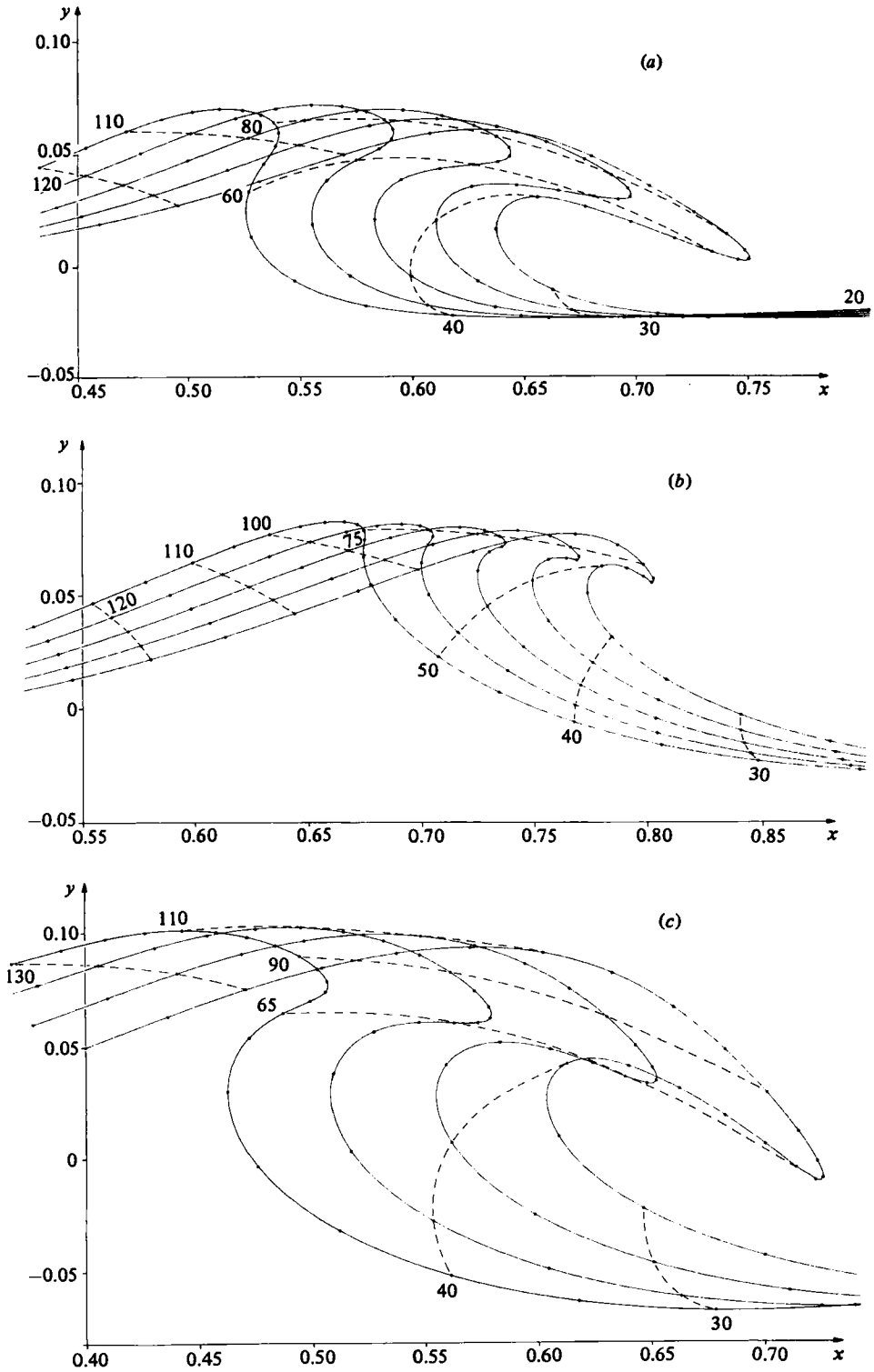

FIGURE 7. Profiles from the high-resolution computations of waves 1 (*a*), 3 (*b*) and 9 (*c*) (times as given in the text): ——, wave profiles; – – – – –, particle paths.

in figures 8(*a–c*). The abscissa and ordinate represent respectively the horizontal (u) and vertical (v) velocities in the free surface, and, for clarity of presentation, the individual fluid particle trajectories are now shown as the solid lines. The positions at the chosen times are marked and the particle numbers are placed near the beginning of each trajectory. (Broken lines represent the envelopes of the starting and finishing positions of all such paths.) The most prominent feature of these diagrams is the development of the jet in the bottom right-hand corner. These particles are approaching free fall and have an increasingly negative vertical velocity and an almost-constant horizontal velocity. Further examination reveals that the horizontal velocities in the ejecting jets are between 1.5 and 2 times the phase speed of the linear wave of the same mean depth and wavelength.

The corresponding fluid particle accelerations are plotted in figures 9(*a–c*). Here the axes represent horizontal (a_x) and vertical (a_y) accelerations, and, returning to the convention of figure 7, each solid line is a 'profile' of the accelerations in the free surface at some instant in time. These profiles are numbered in the time sequence as given above, and a dashed line represents a region of significant numerical error. (For wave 3 at time $t = 1.800$, figure 9(*b*), the error is such that the whole profile is omitted.) The near free-fall motion of the jet tip is indicated by the accumulation of particles near the point $(a_x, a_y) = (0, -1)$ as they pass up the forward face of the wave and into the jet (e.g. follow particles 40–60 for wave 1). Also, the growth of a region of high accelerations beneath the base of the overturning jet is in evidence, for example particles 55–65 in the earliest, and particles 35–40 in the latest, profiles in wave 1 (see figures 7(*a*) and 9(*a*)). In particular, we see that accelerations as high as five or six times that due to gravity ($g = 1$) may occur both horizontally and vertically. By way of comparison, we recall that the maximum acceleration in a steadily progressing wave is only $0.5g$!

6. Discussion

The numerical method of Longuet-Higgins & Cokelet (1976), for unsteady waves in deep water, has been extended to account for a horizontal bottom at finite depth. The only essential modification was in the Green's function which was used in the solution of an integral equation for the unknown component of velocity normal to the free surface. For deep water, this Green's function corresponded to a simple logarithmic singularity, whereas for the finite-depth case images were taken in the bed. The resulting integral equation involved only the free surface so that (unlike the method of Vinje & Brevig 1981) computational particles did not need to be placed on the bottom. (We note that Isaacson (1982) has used a similar technique in calculations of the three-dimensional interactions of non-breaking waves with fixed and floating bodies.)

A variety of overturning motions in shallow water has been investigated. The waves were generated by an initial depth perturbation to the horizontal bed, but were related to motions ensuing on a sloping beach. For waves perturbed from the same initial conditions, a regular transition from spilling to plunging waves was achieved as the severity of the perturbation increased, indicating that these two wave types can be considered as members of a single family with continuously changing characteristics. Referring to figure 5 and table 1, it is apparent that a steep beach leads to the development of a large-scale jet and a highly asymmetric plunging breaker, whereas a gentle slope results in a near-symmetric spilling breaker with only a small-scale jet. This agrees with the observed behaviour of natural breaking waves.

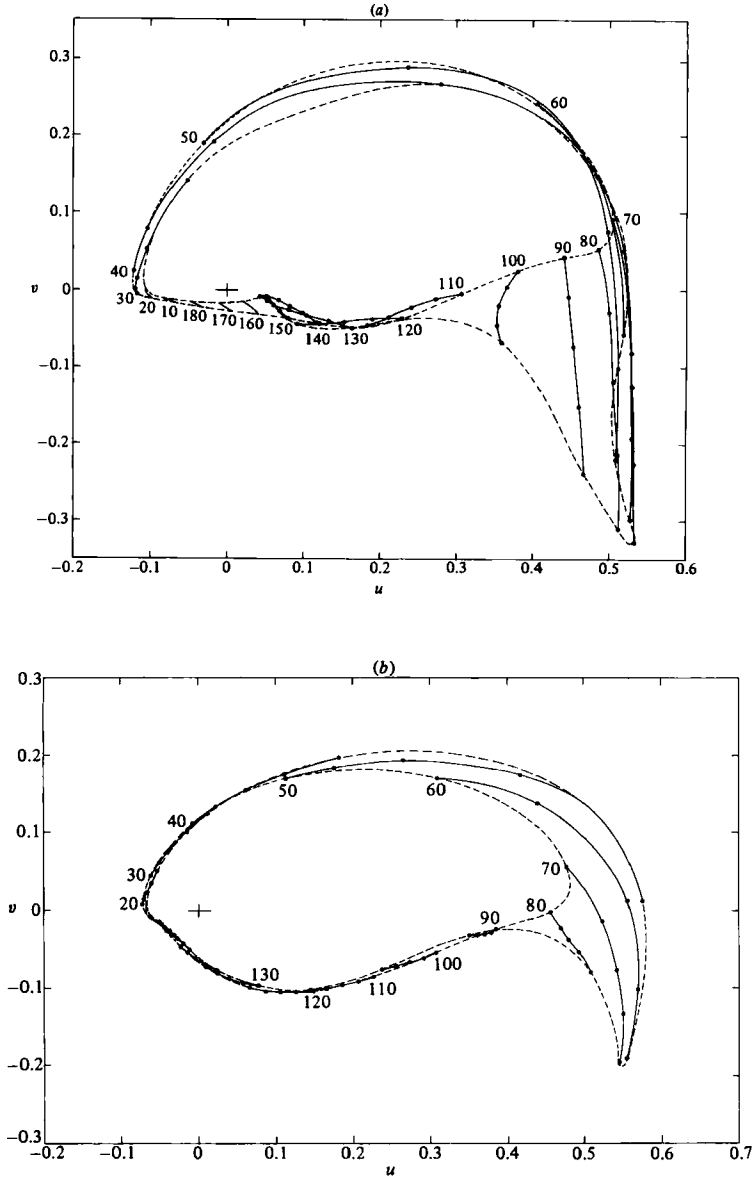

FIGURE 8(*a*, *b*). For caption see opposite.

In spite of a considerable range of global asymmetries in these waves, however, we have noticed that there is typically a strong similarity between the overturning regions. This is illustrated in figure 10, in which the waves, all shown at time $t = t_H$, have been scaled with respect to the jet length S and suitably overlaid (but with no rotation). Wave 1, by far the most severe of the depth-perturbed waves, does not follow the general trend (being too thin), and is excluded; waves 4 and 7 are not shown, because the numerical resolution in the jet region is inadequate. However two examples in which breaking is initiated by a different technique are included: wave 9

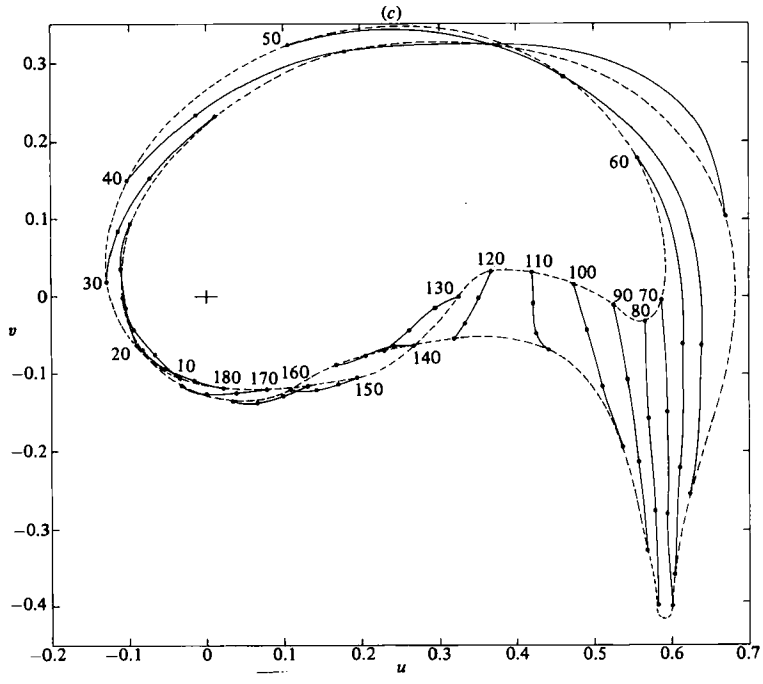

FIGURE 8. Velocity-plane portraits for the high-resolution computations of waves 1 (*a*), 3 (*b*) and 9 (*c*) (times as given in the text): ——, particle trajectories; – – – – –, envelopes of the starting and finishing positions. Particle numbers are indicated at the beginning of each trajectory.

is the breaking sine wave already described, and wave 10 is a 'pressure-forced' wave (see Longuet-Higgins & Cokelet 1976) in which the pressure distribution

$$p_s = -p_0 \sin 2\pi ct \sin 2\pi(x-ct), \tag{6.1}$$

with $p_0 = 0.02$, is applied at the free surface until time $t = 1/2c$ and is thereafter zero. The initial conditions used for this example would represent a steadily progressing wave of height $H_0 = 0.11$ on mean depth $d = 0.2$ (with phase speed $c = 0.40174$) in the absence of the pressure forcing (i.e. if $p_0 = 0$). The similarity between the jet regions of all the waves shown in figure 10 is remarkable, despite the differences in the global asymmetries.

Why such a similarity should exist is not clear, but this has also been hinted at in the computations of both Longuet-Higgins & Cokelet (1978) and Cokelet (1979). However, it may be relevant to remark, as in §5, that it appears as if the jet regions of many waves can be considered as being almost in free fall and dissociated from the body of the wave, so that the evolution of the jet during overturning will be to a large extent independent of the interior dynamics. This striking similarity seems to indicate that a local solution may be valid in the jet region (for instance Longuet-Higgins (1980) suggests that the motion near the jet tip may be described by a rotating form of the Dirichlet hyperbola), and is an incentive for further work to be carried out.

In addition to the present high-resolution computations, velocity- and acceleration-plane plots have also been discussed both by Peregrine *et al.* (1980) and by Baker,

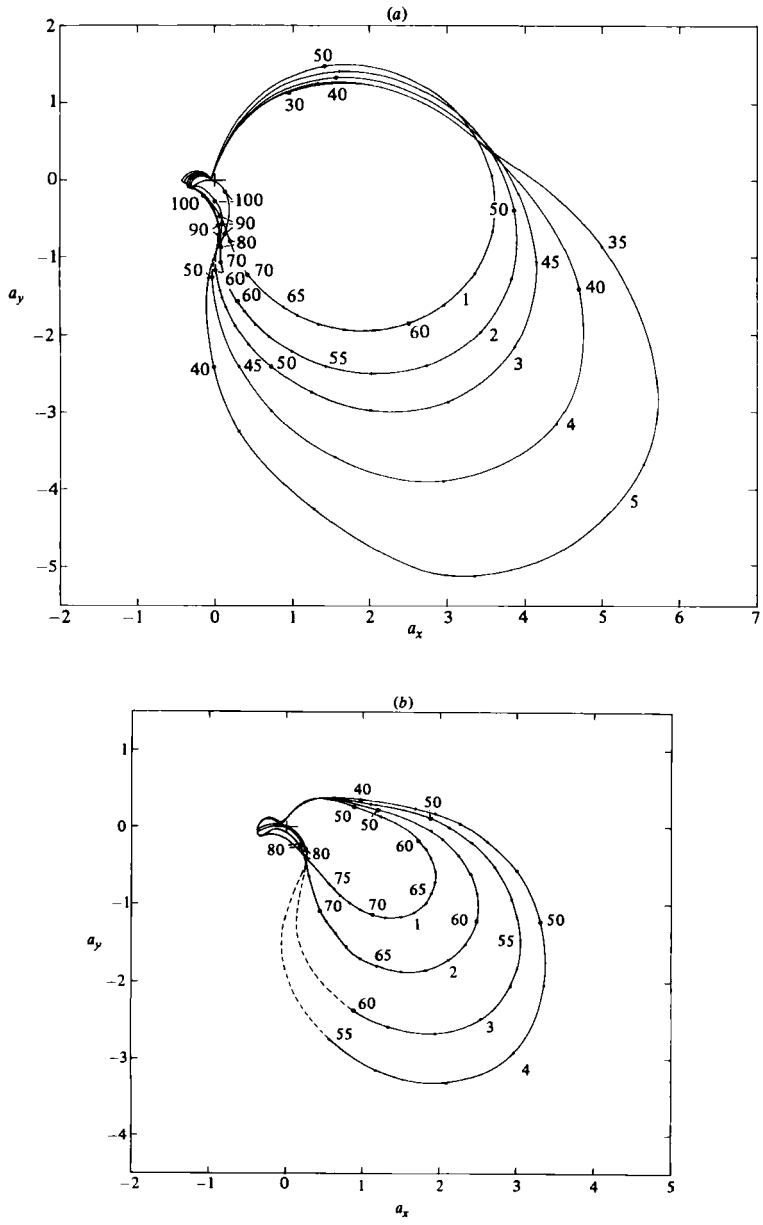

FIGURE 9(*a*, *b*). For caption see opposite.

Meiron & Orszag (1982). However, the computations in the former paper did not proceed until a late stage in the overturning, and only a single example was discussed in the latter. In neither paper could particle trajectories be simultaneously followed through the space, velocity and acceleration planes, so that there seems to be a real need for detailed quantitative information such as is provided by the present computations.

These computations demonstrate that the numerical methods are capable of

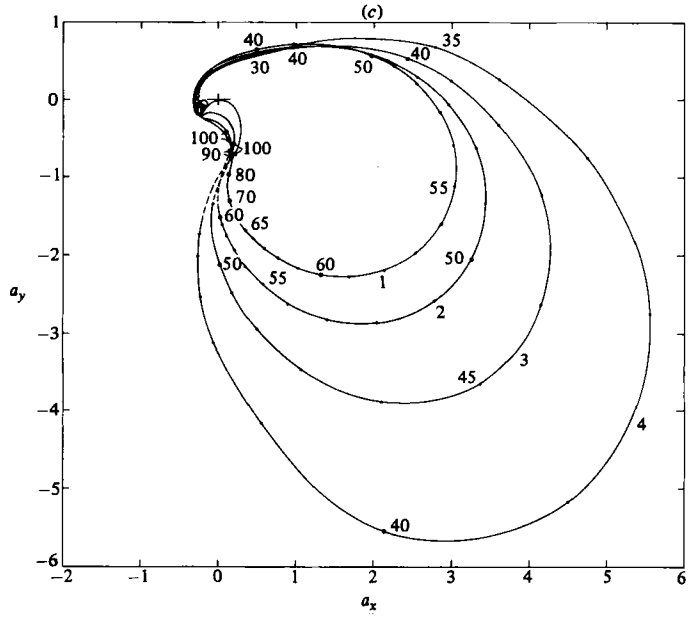

FIGURE 9. Acceleration-plane portraits for the high-resolution computations of waves 1 (*a*), 3 (*b*) and 9 (*c*): ——, envelopes of the free-surface accelerations; – – – – –, regions of unacceptable numerical error. The curves are numbered in the time sequence as given in the text, and the particles are marked as clarity allows (○ identifies every tenth and + every fifth).

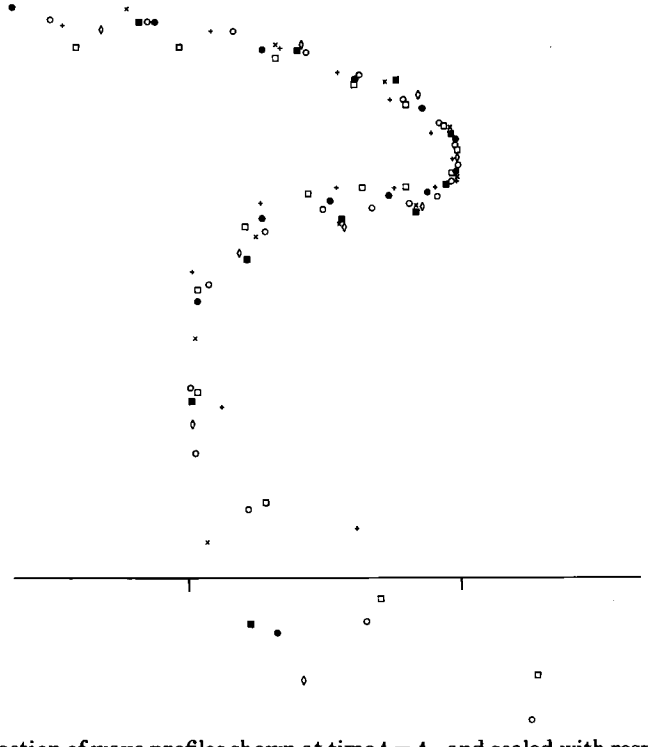

FIGURE 10. A selection of wave profiles shown at time $t = t_H$ and scaled with respect to the jet length S (which is denoted by the tick marks on the arbitrary horizontal axis): ○, wave 2; ●, 3; □, 5; ■, 6; ◇, 8; +, 9; ×, 10.

describing the overturning process from a symmetric wave until the instant when the jet is about to 'touchdown' on the forward face. The 'tube' which forms beneath the projecting jet has itself received considerable attention, with analytical models being proposed by Longuet-Higgins (1982), New (1983*b*) and Greenhow (1983). Although much still remains to be done, high-resolution computations, like those presented here, can provide a valuable check on the validity of the various models.

It is also hoped that the detailed information given (to the authors' knowledge for the first time) in the present paper will be of interest to those concerned with the design of shipping and coastal structures. The growth of a region of high accelerations, for example, is in evidence beneath the base of the overturning region. The pressure gradient in this region of the free surface (and elsewhere) can be easily evaluated from the Euler equation, which, with the present scaling and notation, gives

$$-\nabla p = (a_x, a_y + 1). \tag{6.2}$$

Thus we can verify (from figures 7 and 9) that $-\nabla p$ is always normal to the free surface (upon which p is constant) and that p increases rapidly into the fluid volume (so that instabilities of the Rayleigh–Taylor type should not be present). The high pressure gradients beneath the overturning jet should clearly not be neglected by those concerned with forces on fixed or floating structures in such an environment.

The financial support of the Natural Environment Research Council (A.L.N.) and the Science and Engineering Research Council (P.M.) is gratefully acknowledged.

REFERENCES

BAKER, G. R., MEIRON, D. I. & ORSZAG, S. A. 1982 Generalized vortex methods for free-surface flow problems. *J. Fluid Mech.* **123**, 477–501.

BOWEN, A. J., INMAN, D. L. & SIMMONS, V. P. 1968 Wave set-down and set-up. *J. Geophys. Res.* **73**, 2569–2577.

COKELET, E. D. 1977 Steep gravity waves in water of arbitrary uniform depth. *Phil. Trans. R. Soc.* A **286**, 183–230.

COKELET, E. D. 1979 Breaking waves – the plunging jet and interior flow field. In *Mechanics of Wave-Induced Forces on Cylinders* (ed. T. L. Shaw), pp. 287–301. Pitman.

GALVIN, C. J. 1968 Breaker type classification on three laboratory beaches. *J. Geophys. Res.* **73**, 3651–3659.

GREENHOW, M. 1983 Free-surface flows related to breaking waves. *J. Fluid Mech.* **134**, 259–275.

ISAACSON, M. DE ST Q. 1982 Nonlinear-wave effects on fixed and floating bodies. *J. Fluid Mech.* **120**, 267–281.

LONGUET-HIGGINS, M. S. 1980 On the forming of sharp corners at a free surface. *Proc. R. Soc. Lond.* A **371**, 453–478.

LONGUET-HIGGINS, M. S. 1982 Parametric solutions for breaking waves. *J. Fluid Mech.* **121**, 403–424.

LONGUET-HIGGINS, M. S. & COKELET, E. D. 1976 The deformation of steep surface waves on water. I. A numerical method of computation. *Proc. R. Soc. Lond.* A **350**, 1–26.

LONGUET-HIGGINS, M. S. & COKELET, E. D. 1978 The deformation of steep surface waves on water. II. Growth of normal-mode instabilities. *Proc. R. Soc. Lond.* A **364**, 1–28.

MCIVER, P. & PEREGRINE, D. H. 1981 Comparison of numerical and analytical results for waves that are starting to break. In *Proc. Intl Symp. on Hydrodynamics in Ocean Engineering, Trondheim, Norway*, pp. 203–215.

NEW, A. L. 1983*a* On the breaking of water waves. Ph.D. thesis, University of Bristol.

NEW, A. L. 1983*b* A class of elliptical free-surface flows. *J. Fluid Mech.* **130**, 219–239.

PEREGRINE, D. H., COKELET, E. D. & MCIVER, P. 1980 The fluid mechanics of waves approaching breaking. In *Proc. 17th Conf. Coastal Engineering*, pp. 512–528. ASCE.

RIENECKER, M. M. & FENTON, J. D. 1981 A Fourier approximation method for steady water waves. *J. Fluid Mech.* **104**, 119–137.

VINJE, T. & BREVIG, P. 1981 Numerical calculations of forces from breaking waves. In *Proc. Intl Symp. on Hydrodynamics in Ocean Engineering, Trondheim, Norway*, pp. 547–565.